A conserved stripe rust effector elicits variable resistance responses in wheat

Eric C. Pereira[1‡], Bayantes Dagvadorj[1‡], Rita Tam[1], Haoran Li[1], Danish Ilyas Baig[1], Mareike Möller[1], Miraclemario Raphael[1], Simon Williams[1], Sambasivam Periyannan[1,2,3], Florence Danila[1], John P. Rathjen[1], and Benjamin Schwessinger[1]

[1]Research School of Biology, The Australian National University, Canberra, ACT, 2601 Australia

[2]Commonwealth Scientific and Industrial Research Organisation Agriculture and Food, Canberra ACT 2601, Australia

[3]School of Agriculture and Environmental Science, Centre for Crop Health, University of Southern Queensland, Toowoomba QLD 4350, Australia

***Corresponding author:** *benjamin.schwessinger@anu.edu.au*

Abstract

Plant resistance (*R*) and pathogen avirulence (*Avr*) gene interactions are central to pathogen recognition and disease resistance in crops. However, functional characterisation of *Avr* effectors in *Puccinia striiformis* f. sp. *tritici* (*Pst*) remains challenging due to its obligate biotrophic lifestyle. Here, we used a high-throughput wheat protoplast-based screen to evaluate *Avr*/*R* interactions efficiently, enabling rapid detection of effector-induced defence responses across diverse wheat cultivars. We identified an *Avr* candidate that we termed *AvrPstB48* as a defence-

activating effector, consistently triggering defence responses in 16 out of 24 independent wheat cultivars tested. *AvrPstB48* is hemizygous, and the *Pst* genome carries four divergent paralogs within a single gene cluster on separate haplotypes. Analysis of these paralogs revealed partial redundancy in their abilities to activate wheat defences and enabled us to identify a single amino acid in *AvrPstB48,* which is necessary but not sufficient for defence activation. Notably, the activation of defence by *AvrPstB48* in protoplasts did not consistently translate into resistance *in planta*. Whole-plant infection assays revealed that some cultivars that exhibited strong defence activation in the protoplast assay remained fully susceptible to *Pst*. However, comparison of infection dynamics between the *AvrPstB48*-recognising cultivar Avocet S and the non-recognising susceptible cultivar Morocco revealed a delay in disease progression in Avocet S, evidenced by reduced mycelial growth and increased callose deposition at 10 days post-inoculation. This supports the hypothesis that while *AvrPstB48* is recognised by specific host genotypes, its immune activation is actively suppressed *in planta* by additional *Pst*-encoded suppressor effectors.

Keywords: *Puccinia striiformis* f. sp. *tritici*, effectors, avirulence genes, protoplast screening, wheat resistance, plant immunity.

INTRODUCTION

Plant pathogenic fungi are major contributors to crop losses globally, with diseases such as wheat stripe rust caused by *Puccinia striiformis* f. sp. *tritic*i (*Pst*) continuing to impact wheat production worldwide, driven by ongoing intercontinental spread and

genetic diversification (Hovmøller et al., 2010; 2025). The infection strategy of this fungus includes the secretion of large sets of so-called effector proteins into plant tissue (Wang et al., 2023). Such effectors modulate host cellular processes to suppress defence responses and enhance pathogen colonisation (Zheng et al., 2023). Identification of recognised effectors and their functional characterisation are aspects towards advancing management strategies.

A subset of effectors designated avirulence (*Avr*) effectors are detected by resistance (*R*) genes in certain host genotypes (Xia et al., 2020). *Avr* recognition triggers a myriad of defence responses, including transcriptional reprogramming that restricts pathogen colonisation (Dodds & Rathjen, 2010). Several *Avr* genes from wheat rust fungi have been cloned. For example, cloning of *Avr* genes from *P. graminis* f. sp. *tritici* (*Pgt*), including *AvrSr50* (Chen et al., 2017), *AvrSr35* (Salcedo et al., 2017), *AvrSr27* (Upadhyaya et al., 2021; Outram et al., 2024), *AvrSr62* (Chen et al. 2024), *AvrSr22* and *AvrSr13* (Arndell et al., 2024), has provided detailed insights into pathogen recognition. Similar advances have been reported for *Blumeria graminis*, with the identification of *AvrPm2* (Praz et al., 2017) and *AvrPm3* (Bourras et al., 2019), and *Zymoseptoria tritici* fungi, with the identification of *AvrStb6* (Zhong et al., 2017), *Avr3D1* (Meile et al., 2018), *AvrStb9* (Amezrou et al., 2023) and *Zt-11* (Karki et al., 2024). Additionally, recent studies in *P. triticina* have identified novel effectors that may play key roles in virulence and host specificity, such as *Pt1641* (Chang et al., 2024), *AvrLr21* (Shen et al., 2024) and *AvrLr15* (Cui et al., 2024).

Many immune recognition events in plants are mediated by intracellular receptors known as nucleotide-binding leucine-rich repeat (NLR) proteins, which are often encoded by *R* genes. Upon recognising specific Avr effectors, NLRs initiate downstream defence responses such as transcriptional reprogramming and

programmed cell death. Some effectors interfere with shared immune signalling nodes that integrate pattern recognition receptor (PRR) and NLR-mediated responses or modulate host metabolic pathways to subvert immunity (Ramírez-Zavaleta et al., 2022; Rhodes et al., 2022). Thus, effectors not only activate immune responses but can suppress them, leading to effector-triggered susceptibility (ETS) (Win et al., 2012). These highlight the dual roles of effectors in virulence and immunity and the complex interplay of recognition and suppression in plant-pathogen interactions.

Despite significant progress in cloning wheat *R* genes, the identification of corresponding *Avr* genes in rust fungi has lagged, largely due to the pathogen's dikaryotic genome organisation and obligate biotrophic nature, which hinders *in planta* functional studies (Wang et al., 2023; Li et al., 2024; Running & Faris, 2024). This limits our understanding of how effector-*R* gene interactions shape phenotypic variation among *Pst* pathotypes and influence virulence evolution (Norman et al., 2023). To overcome these challenges, we adapted and optimised a high-sensitivity protoplast-based screening system for functional testing of *Pst* effector candidates. Building on the methodology described by Wilson et al. (2024), we incorporated the self-replicating pWDV1 vector system to enhance transient expression of luciferase reporters linked to defence activation. This optimisation significantly improved signal-to-noise ratio, reduced DNA input requirements, and increased assay throughput, enabling scalable and reliable detection of Avr/R interactions in wheat protoplasts. Thus, this platform allows detection of *Avr*-triggered immune responses in wheat cells, bypassing the limitations of whole-plant assays (Saur et al., 2019; González-Grandío et al., 2021; Lubega et al., 2024). Using a fully phased genome assembly of the Australian *Pst* isolate 104E137A-, where both haploid nuclear genomes are

independently resolved, it has become possible to identify effector genes that are hemizygous, i.e. present in only one of the two haploid nuclei. These single-copy effectors are of particular interest because hemizygosity may reflect selective pressure to evade host recognition, representing an early stage in stepwise virulence evolution. By screening such candidates, we aimed to identify effectors with a high likelihood of avirulence activity that may be differentially recognised by specific wheat genotypes and potentially contribute to gene-for-gene resistance dynamics.

This study characterises an evolutionary conserved *Pst* effector using a protoplast screening system and diverse wheat lines. In addition to confirming its recognition, we analysed the effector's sequence diversity, expression patterns during infection, and its impact on host defence responses. Our findings advance the understanding of how recognition and suppression interplay in the *Pst*–wheat pathosystem, providing insights into the evolution of pathogen virulence and strategies for durable resistance deployment.

MATERIAL AND METHODS

Candidate *Pst Avr* selection and gene synthesis

Avr candidates were previously identified by analysing a time course of long-read transcriptomic datasets of *Pst*104E137A-, as detailed in Tam et al. (2025). Briefly, the transcripts were sampled from six conditions with four replicates each, including ungerminated urediniospores and infected wheat leaves at 4, 6, 8, 10, and 12 days post-infection (dpi). All samples were subjected to direct Oxford Nanopore Technologies (ONT) cDNA sequencing. DESeq2 (Love et al., 2014) differential expression analysis was conducted on transcript read abundance to identify secretome genes upregulated ($\log_2$ fold change ≥ 2) early during infection (4 and 6

dpi) relative to dormancy. Inter-haplotype sequence analysis was then conducted to shortlist the candidates based on hemizygosity. The selected candidates were synthesised as gene blocks to facilitate precise assembly through Golden Gate cloning (Engler et al., 2014).

Identification of *AvrPstB48* paralogs

tblastn v2.16.0+ was used to search for *AvrPstB48* paralogs using its translated protein sequence against the *Pst*104E genome assembly (-evalue 1e-5). We applied a low identity cut-off of 0.4, considering effector proteins are typically sequence-divergent yet structurally conserved (Yu et al., 2023). The search results were used to locate the annotated gene hits. Multiple protein sequence alignments were performed using MAFFT v7.490 (Katoh & Standley, 2013) and visually inspected in Geneious to confirm overall similarities in physicochemical properties despite residue substitutions.

***In silico* structural modelling**

The predicted tertiary structures of *AvrPstB48* and its paralogs were generated using the AlphaFold Server v3.0 (DeepMind, UK) (Abramson et al., 2024). Models were generated based on the protein sequences with the signal peptides removed. The predicted Template Modelling (pTM) score can be used to assess global model quality and domain orientation, where scores ≥0.5 are generally considered acceptable for reliable domain-level predictions (Jumper et al., 2021). The initial scores for all structural models were <0.5 (Supplementary Table S1). However, we observed from those models that ~50 residues at the N-terminus of each protein were unstructured. We also noted that the sequences of the proteins were rich in

conserved cysteine residues. In other rust effectors, these have been shown to co-ordinate Zn^{2+} (Zhang et al., 2018; Outram et al., 2024). We therefore repeated the predictions with the N-terminal truncated and Zn included. We observed an overall improvement in the pTM scores for all models >0.5 when the N-terminal region was removed, and this was generally improved when Zn was added to the prediction. The interface prediction score for Zn binding was in most cases >0.7, indicating acceptable interaction reliability (Abramson et al., 2024) (Supplementary Table S1). The resulting models were visualised and analysed using ChimeraX v1.8 (UCSF) (Meng et al., 2023). Structural comparison of *AvrPstB48* and its paralogs (P1, P2/P4, and P3) was performed via superimposition, using *AvrPstB48* as the reference structure to identify conformational differences that may underlie functional divergence.

Golden Gate assembly of expression constructs

The hemizygous effector candidate gene ID *Pst104E137_010232* (*AvrPstB48*), its paralogs *Pst104E137_025766* (*AvrPstB48*_P1), *Pst104E137_025767* (*AvrPstB48*_P2), *Pst104E137_010231* (*AvrPstB48*_P3), and the mutants *AvrPstB48*_D133G and *AvrPstB48*_P3_G133D were digested with the *BsaI* restriction enzyme, creating compatible seamless overhangs. Simultaneously, the digested fragments were ligated into the *pWDI* expression vector, which had also been digested with *BsaI*. The reaction was cycled between 37°C for 3 minutes (to allow digestion) and 16°C for 4 minutes (for ligation) for 25 cycles, followed by a final incubation at 50°C for 5 minutes and 80°C for 5 minutes to inactivate the *BsaI* enzyme.

Following the Golden Gate reaction, 5 µL of the reaction mixture was transformed into competent *E. coli* cells. The cells were incubated on ice for 30 minutes, heat-shocked at 42°C for 30 seconds, and then returned to ice for 5 minutes. SOC medium (200 µL; containing 2% tryptone, 0.5% yeast extract, 10 mM NaCl, 2.5 mM KCl, 10 mM $MgCl_2$, 10 mM $MgSO_4$, and 20 mM glucose) was added, and the mixture was incubated at 37°C for 1 hour with shaking at 250 rpm.

Transformed *E. coli* cells were plated on LB agar supplemented with 35 µg/mL chloramphenicol and incubated overnight at 37°C. Individual colonies were screened by colony PCR using gene-specific primers to confirm the presence of *Avr* candidate inserts (Supplementary Table S2). PCR-positive clones were cultured in LB broth for plasmid extraction using a standard miniprep protocol (Qiagen). Extracted plasmids were subjected to restriction enzyme digestion with insert-specific restriction sites to validate correct plasmid architecture. Clones showing the expected digestion patterns were then selected for full-length plasmid verification via ONT sequencing. Whole-plasmid sequencing was performed using ONT MinION flow cells, and raw reads were analysed in Geneious Prime v2025.1.3 using Minimap alignment against the plasmid reference map to confirm correct insert orientation, sequence integrity, and absence of mutations (Li, 2018) (Supplementary Table S3).

Plant materials and growth conditions

Twelve batches of *Pst*-infected plants were used in the study. For each infection batch, 15 seeds each of wheat cultivars (cv) Chinese 166, Avocet/*Yr1*, Heines VII , Nord Desprez, *Triticum spelta*, Avocet/*Yr5*, Heines Peko, Heines Kolben, Avocet/*Yr6,* Reichersberg 42, Avocet/*Yr7*, Compare, Avocet/*Yr8,* Clement, Avocet/*Yr9*, *Yr15*, Avocet/*Yr15*, Spalding prolific, Avocet/*YrSp*, Avocet S, Breakwell, Gabo, Coorong

and Morocco were sown in each pot (14 cm in diameter, 10 cm in depth, and approximately 1.5 L in volume), with 6 pots set for each tray. Two trays were prepared for the treatment group, and one tray was prepared for the control group. The control and treatment groups were grown in separate growth cabinets (18°C, 16 h photoperiod, 300 μmol/m²/s light intensity, 60% relative humidity from 7 am and 70% relative humidity from 11 pm). Ten grams of soluble fertiliser (HORTICO) was dissolved in 4.5 L of water, and 2.25 L was applied to each tray of plants. 100 mL of growth inhibitor (0.5% maleic hydrazide in Milli-Q water) was applied to each tray 8 days after sowing. Plants were watered every three days.

Protoplast isolation

Wheat protoplasts were isolated using the protocol described by Wilson et al. (2023, 2024), with minor modifications. Briefly, wheat cultivar plants were grown under controlled conditions in a growth cabinet for 7 to 9 days. Protoplast isolation was achieved by making shallow incisions on the leaf epidermis and then peeling the epidermal layer to reveal the underlying mesophyll cells. The excised leaf segments were then incubated with the peeled surface in contact with a 0.6 M mannitol solution for 10 minutes. Subsequently, the segments were transferred to a well of a 12-well cell plate (2.3 cm) containing a filtered enzyme solution composed of MES buffer (pH 5.7, 20 mM), mannitol (0.8 M), KCl (10 mM), cellulase (Yakult R-10) 1.5% w/v, macerozyme (Yakult R-10) 0.75% w/v, CaCl2 (10 mM), and BSA 0.1% w/v. The plate was wrapped in aluminium foil to prevent light exposure and placed on an orbital shaker set to 60 RPM for 3 hours. The enzyme solution was filtered, and the protoplasts were then collected by gentle centrifugation at 100 g for 3 minutes using a 14 mL round-bottom tube (17/100 mm). The enzyme solution was decanted, and

the protoplast pellet was rinsed with W5 solution (MES buffer, pH 5.7, 2 mM; KCl, 5 mM; $CaCl_2$, 125 mM; NaCl, 154 mM). Using a hemocytometer and light microscope, a 10 µl aliquot of the concentrated protoplasts was taken for cell quantification and quality assessment. The protoplasts were left at 4°C for 40 minutes to allow settling. The W5 solution was then removed, and the protoplasts were resuspended to a concentration of 300,000–350,000 cells/mL using MMG solution (MES buffer, pH 5.7, 4 mM; mannitol, 0.8 mM; $MgCl_2$, 15 mM). The protoplasts were used immediately for subsequent transfection.

Protoplast transfection

Plasmid DNA (1 µg/µL) was prepared using standard mini- and maxi-prep protocols (Promega SV Wizard, Madison, WI, USA). The protoplast transfection protocol based on the method developed by Wilson et al. (2024) was adapted to a 96-well plate format to increase scalability and throughput. A wheat codon-optimised luciferase reporter gene (Luc) was cloned into the pWDV1 self-replicating vector under the control of the maize ubiquitin (UBI) promoter to enhance expression levels. Similarly, all *Avr* candidates and *R* genes were expressed from the same UBI promoter system in pWDV1 constructs.

For each transfection replicate, the following DNA amounts were used: 0.5 µg of *Avr* plasmid, 10 µg of *R* gene plasmid, and 5 µg of the luciferase reporter plasmid. For *Avr*-only transfections, 1 µg of *Avr* candidate plasmid and 5 µg of luciferase plasmid were used. Plasmid DNA was pipetted into individual well of 96-well V-bottom plates (Costar). To each well, 50 µL of freshly isolated wheat protoplasts and 50 µL of PEG solution (40% w/v PEG 4000, 0.2 M mannitol, 100 mM $CaCl_2$) were added and gently mixed by pipetting up and down five times. Samples were incubated for 10

minutes at room temperature to allow for transfection, after which 200 µL of W5 solution (154 mM NaCl, 125 mM $CaCl_2$, 5 mM KCl, 2 mM MES, pH 5.7) was added to stop the PEG-mediated uptake. Following an additional one-hour incubation with protoplasts settled at the bottom of the well, the supernatant was removed, and the protoplasts were carefully resuspended in 200 µL of fresh W5 solution. The cells were incubated under low-light conditions at room temperature for 16 h to allow gene expression prior to luciferase quantification.

Monitoring luciferase expression

After the incubation, the protoplasts were prepared for luminescence measurement. The W5 supernatant was removed using a multichannel pipette, taking care not to disturb the protoplast pellet. 50 µL of 1× cell lysis buffer (#E3971; Promega) was added, and the samples were gently mixed by pipetting 5 times, followed by a 15-minute incubation. 50 µL of lysate was collected and transferred to an opaque, flat-bottom, white, solid polystyrene 96-well plate (Corning 96-well NBS Microplate, #CLS3600). The total luminescence was measured using a plate reader (Tecan, Mannedorf, Switzerland; Infinite 200Pro, 1000 ms integration, 0 ms settle) without adding substrate to measure background signal. Then, 50 µl Steady-Glo (#E2520; Promega) Luciferin substrate was added to each well, and the luminescence was measured again. The plate reader was programmed first to measure total luminescence without filters, using an integration time of 1000 ms and a settle time of 0 ms. Subsequently, luminescence was measured well-wise using green and red filters under the same acquisition settings.

Inoculation of wheat plants with *Pst*

Fresh spores of *Pst* isolate 104E137A- (Schwessinger et al., 2018) were collected from infected leaf tissue. Spores were suspended in 3M Novec solution and measured using a CellDrop Automated Cell Counter (DeNovix Inc.) to a concentration of approximately 5×10^5 spores/mL. Using a paintbrush, spores were inoculated on the upper surface of the first-emerged leaf of wheat plant 14 days after sowing. Infected plants were lightly sprayed with clean deionised water before being placed in an opaque, 25-L plastic container with lid (33 cm x 22.5 cm x 47 cm) and filled with water to 25% capacity. Containers with infected plants were wrapped with black plastic bags and incubated at 10°C in the dark to initiate *Pst* germination. After 48 hours, the infected plants were removed from the container and transferred back to the growth cabinet. Each infected leaf was assessed according to Dracatos et al. (2016) over 10 or more days post-infection (dpi).

Hyphae staining of infected wheat leaves

Staining was performed as described by Redkar *et al.* (2018). Freshly harvested leaf tissues were placed in 2 mL tubes containing 100% ethanol for three days or until majority of the chlorophyll had been removed. When the tissues were nearly devoid of colour, ethanol was replaced with 10% aqueous potassium hydroxide and incubated on a dry heating block at 85°C for two hours. Cleared tissues were carefully washed 10 times in 1x phosphate-buffered saline (PBS Thermo Fisher Scientific, 28237), pH 7.4. Propidium iodide (PI; Sigma-Aldrich, P4170) was mixed with wheat germ agglutinin conjugated with AlexaFluor488 (WGA-AF488; Thermo Fisher Scientific, W11261) to create a PI-WGA AF488 staining solution (20 µg/mL PI, 10 µg/mL WGA-AF488, and 0.1% Tween 20 in 1× PBS, pH 7.4). After discarding the last PBS wash, PI-WGA-AF488 staining solution was added to the 2 mL tubes to

fully submerge the tissues. Vacuum infiltration was applied at 7 millibars, repeated 5 times for 2 minutes each, with 2-minute vacuum release in between. Stained tissues were washed twice in 1x PBS to remove excess staining solution, transferred to fresh 1x PBS and stored at 4°C in the dark.

Callose staining of infected wheat leaves

Freshly harvested leaf tissues were placed in 2 mL tubes containing 1x PBS, pH 7.4 and vacuum infiltrated at 7 millibars until they sank to the bottom of the tube. Prior to staining, leaf tissues were hand-sectioned paradermally using a razor blade. Eight pieces of sectioned leaf tissue were placed in each well of the 96-well plate and washed with 200 µL 1x PBS. Tissues were stained with 0.1% aniline blue (AB; Sigma-Aldrich, 415049) in 1x PBS for 60 mins with vacuum infiltration and washed twice in 1x PBS. WGA-AF488 staining solution (10 µg/L WGA-AF488 and 0.1% Tween 20 in 1× PBS, pH 7.4) was added to the samples and vacuum infiltrated at 7 millibars for 5 times, 2 minutes each, with 2-minute vacuum release in between. Samples were washed twice in 1x PBS, transferred to fresh 1x PBS and stored at 4°C in the dark.

Confocal fluorescence microscopy

Stained leaf tissues were mounted onto a glass slide with 1x PBS and imaged under a TCS SP8 confocal microscope (Leica Microsystems) using 20x (PI-WGA-AF488) and 63x (AB-WGA-AF488) water-immersion objectives. WGA-AF488-stained fungal structures was visualised at 500-540 nm following excitation with an Argon laser at 488 nm. PI-stained cell wall was visualised at 580-630 nm following excitation with a

DPSS laser at 561 nm. AB-stained callose was visualised at 430-500 nm following UV excitation at 405 nm. To obtain a composite image with greater depth of field, Z-stacking was performed with each optical section captured at 0.1 µm interval. Images were processed (e.g., maximum projection, brightness and contrast) using Leica Application Suite X software (LASX, Leica Microsystems).

Data collection and statistical analysis

Differences in normalised luminescence values were assessed using one-way analysis of variance (ANOVA) followed by Tukey's Honestly Significant Difference (HSD) post hoc test (Wilson et al., 2024). The infectious hyphae cover area per leaf surface area was quantified using images obtained from PI-WGA-AF488-stained leaf tissues. Meanwhile, the callose signal area was quantified using images obtained from AB-WGA-AF488-stained leaf tissues. These quantifications were performed using ImageJ software (National Institutes of Health) on a Wacom Cintiq graphics tablet (Wacom Technology). Statistical analysis of data obtained from confocal images was performed using Welch's t-test.

RESULTS

A conserved stripe rust candidate effector triggers defence signalling in wheat protoplasts

The Avr candidates were sourced from previous work on the nuclear haplotype-phased genome of isolate *Pst*104E (Tam et al., 2025). The candidate genes were identified based on the predicted presence of an N-terminal signal peptide, absence of a transmembrane domain in the mature protein sequence, as well as

transcriptional upregulation during early wheat infection. From this set of candidate effectors, we identified and functionally uncharacterised *AvrPstB48* as an effector candidate. The name *AvrPstB48* reflects its predicted avirulence function “Avr” in *Pst*, with “B” representing its broad recognition pattern across diverse wheat cultivars, and “48” corresponding to its internal candidate ID in the screening pipeline.

Based on this candidate prioritisation pipeline, we selected a panel of high-confidence effector candidates for functional validation in wheat protoplasts. Additional candidates, including *Pst104E137_008104* (#47) and *Pst104E137_024713* (#49), were selected using the same criteria and served as comparisons for validation assays.

Using a luciferase-based reporter assay under the control of the D14 defence promoter (Wilson et al., 2024), we observed a robust and specific increase in ratiometric luminescence following co-expression of *AvrPstB48* and the defence reporter, indicating a recognition-dependent defence response in Avocet *Yr5* and Avocet S (Figure 1). The increase in ratiometric luminescence observed in *AvrPstB48* was consistent with the *AvrSr50/Sr50* gene pair, which served as a positive control to validate the assay performance (Supplementary Table S4) (Wilson et al., 2024). By contrast, other hemizygous candidates, #47 and #49, did not induce measurable reporter activity similar to negative control, AvrSr50 (Figure 1). Together, these results are consistent with *AvrPstB48* encoding a recognised effector capable of activating host defence responses in specific wheat backgrounds (Supplementary Table S5).

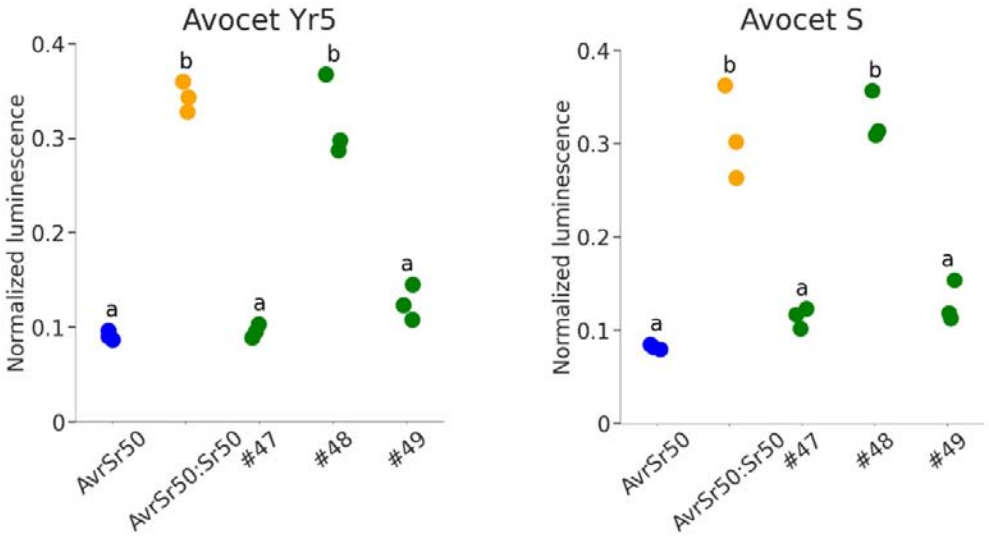

Figure 1 –*pDefense* D14 promoter activation triggered by *AvrPstB48* in Avocet *Yr5* and Avocet S protoplasts. Luciferase-based reporter assays were performed using wheat protoplasts from cultivars Avocet *Yr5* and Avocet S to assess defence signalling. The x-axis shows the plasmid combinations tested, including candidate effectors *Pst104E137_008104* (#47), *Pst104E137_010232* (*AvrPstB48*), and *Pst104E137_024713* (#49), along with the positive control pair *AvrSr50/Sr50*. The y-axis represents normalised luminescence values, measured as the ratio of luciferase activity driven by the D14 promoter to the internal control UBI-pRed. *AvrPstB48* triggered a significant increase in reporter activity, indicating activation of defence responses. Statistical differences were analysed using one-way ANOVA followed by Tukey's Honestly Significant Difference (HSD) test; treatments sharing a common letter are not significantly different ($p > 0.05$).

Given the strong defence promoter activation observed for *AvrPstB48*, further analysis was conducted to identify and characterise its paralogs. Sequence homology analysis were performed by tblastb and revealed two divergent paralogs located in close proximity on each haplotype of chromosome 10, *AvrPstB48*_P1, *AvrPstB48*_P2, *AvrPstB48*_P3 and *AvrPstB48*_P4. Among these, *AvrPstB48*_P2 and *AvrPstB48*_P4 share 100% nucleotide identity, whereas *AvrPstB48*_P1 and *AvrPstB48*_P3 exhibit 98.2% nucleotide identity (Figure 2a). The translated protein

sequence alignment revealed substantial divergence in *AvrPstB48*_P1 and *AvrPstB48*_P3 relative to *AvrPstB48*, whereas *AvrPstB48*_P2/P4 exhibited high sequence conservation (Figure 2b). Structural modelling using AlphaFold predicted that *AvrPstB48* and its paralogs (P1, P2/P4, and P3) adopt broadly conserved three-dimensional architectures, characterised predominantly by α-helical folds (Figure 2c). Despite overall structural similarity, subtle differences in surface-exposed regions and loop conformations may underlie functional divergence and differential interaction with host targets. These predicted structural variations are consistent with the amino acid substitutions observed in the multiple sequence alignment (Figure 2b), particularly in regions that may influence effector recognition or stability within the host environment. Temporal expression profiling across infection stages revealed distinct expression patterns among the paralogs (Figure 2d). *AvrPstB48* exhibited peak expression at 8 days post-inoculation (dpi), reaching its highest levels relative to the other paralogs. In contrast, *AvrPstB48*_P1 was strongly expressed at 4 and 6 dpi but declined thereafter, suggesting an early role in infection. *AvrPstB48*_P2/P4 and *AvrPstB48*_P3 displayed moderate expression at later time points, while none of the paralogs were expressed in ungerminated spores, supporting their likely function in host-pathogen interactions.

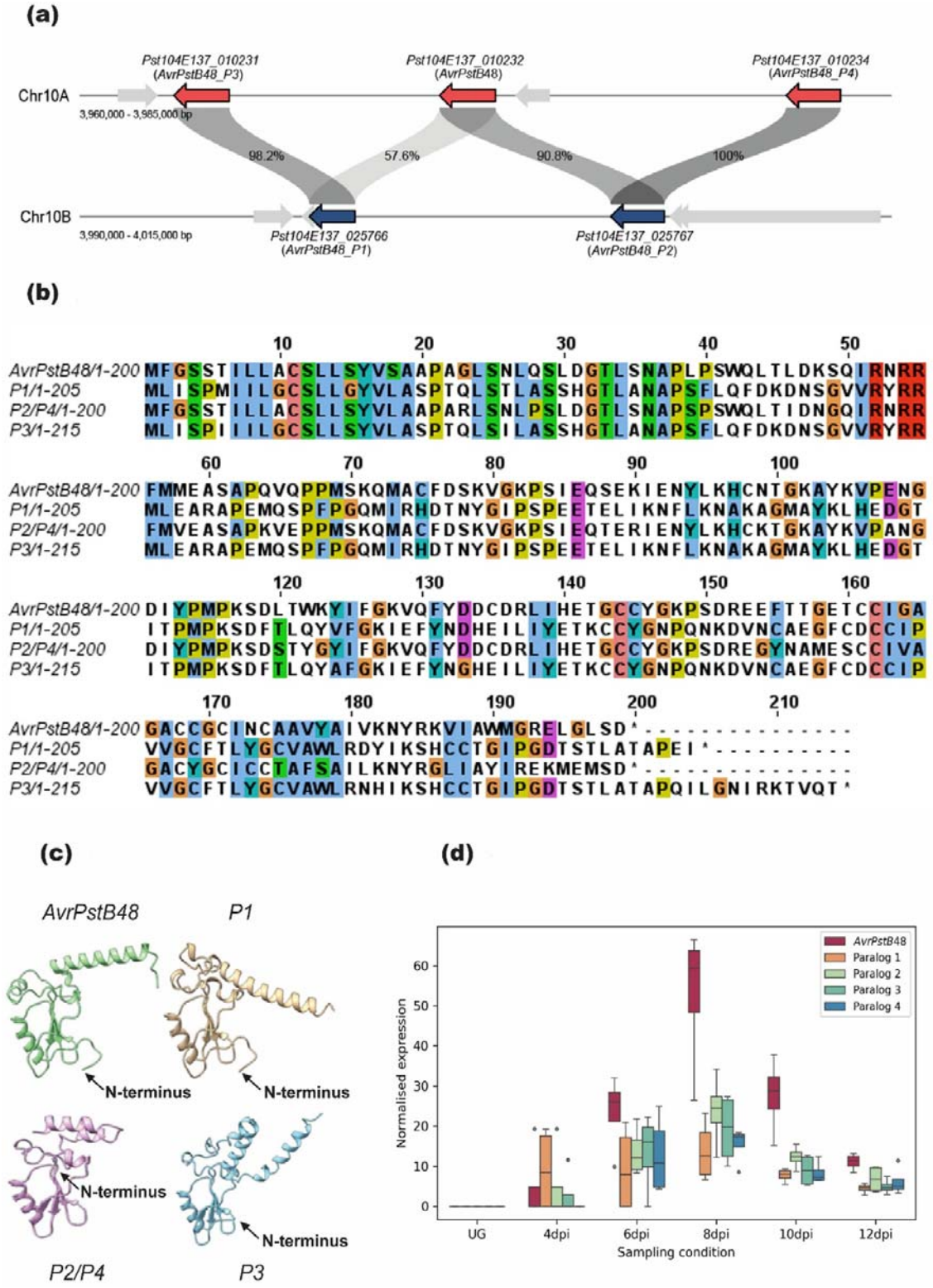

Figure 2 – Genomic, evolutionary, and structural characterisation of the candidate effector gene *AvrPstB48* and its paralogs. (a) Genomic organisation and synteny of *AvrPstB48* (*Pst104E137_010232*, red arrow) and its paralogs (P1: *Pst104E137_025766*; P2:

Pst104E137_025767; P3: *Pst104E137_010231*; P4: *Pst104E137_010234*) across homologous regions of Chromosomes 10A (highlighted as red arrows) and 10B (highlighted as blue arrows). Grey shaded blocks represent pairwise nucleotide sequence identity between corresponding regions, with percentages denoting the degree of similarity. **(b)** Multiple sequence alignment of AvrPstB48 and its paralogs, showing conservation at the amino acid level. Identical or similar residues are highlighted using the Clustal X colour scheme, which assigns colours based on amino acid conservation and physicochemical properties using threshold criteria. Conserved motifs are evident across the sequences. Dashes indicate gaps in the alignment. **(c)** Predicted 3D structures of *AvrPstB48* and its paralogs generated using AlphaFold3. Structural models suggest all paralogs share an overall conserved fold**. (d)** Expression profile of *AvrPstB48* and its paralogs (Paralog 1, Paralog 2, Paralog 3) at dormancy (ungerminated urediniospores) and different infection stages (days post-inoculation, dpi) *in planta*, revealing stage-specific transcriptional dynamics. Expression was normalised and plotted as box plots with biological replicates.

AvrPstB48 **recognition is conserved across multiple wheat cultivars**

To further assess defence promoter activation triggered by *AvrPstB48* and its paralogs, we tested their activities in additional wheat cv. including Avocet S, Morocco, *Triticum spelta Yr5*, Chinese 166 and Gabo, using three previously validated defence-associated promoters (D2, D14, and D15) (Wilson et al., 2024). Significant activation of each promoter was observed in response to *AvrPstB48* expression in Avocet S (Figure 3a), *T. spelta Yr5* and Gabo (Supplementary Figures S1a, S1b), indicating conserved recognition of this effector. In contrast, no detectable luminescence signal was detected in cvs Morocco (Figure 3b) or Chinese 166 (Supplementary Figure S1c), suggesting a lack of *AvrPstB48* recognition in these cultivars. Additional screening of 16 wheat cultivars confirmed consistent activation in all Avocet near-isogenic lines, while eight cultivars showed no measurable response (Supplementary Table S5). Importantly, the positive control (*AvrSr50/Sr50*)

consistently induced strong luminescence across all tested backgrounds, validating assay performance, whereas the negative control consistently showed no response.

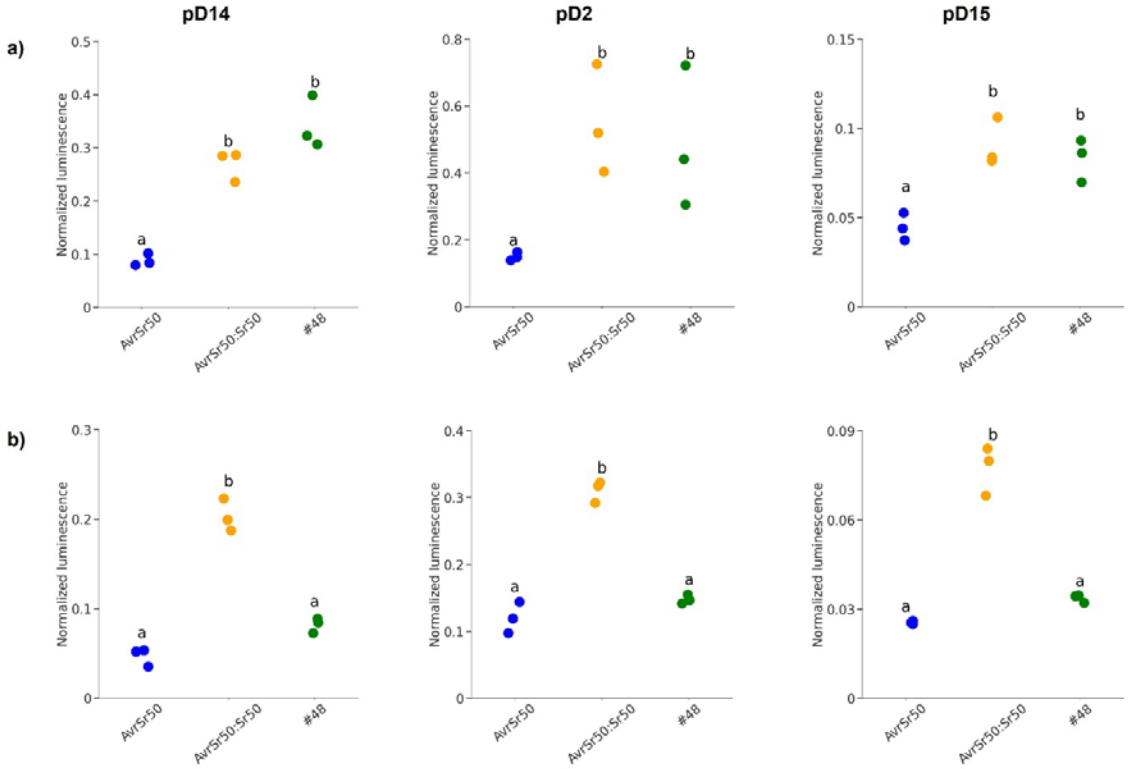

Figure 3 – Differential activation of defence reporters by *AvrPstB48* reveals genotype-dependent recognition. Normalised luminescence signals from protoplast-based defence reporter assays using three promoter constructs (pD14, pD2, pD15) and UBI-pRedf in **(a)** Avocet S and **(b)** Morocco. *AvrSr50* and *AvrSr50:Sr50* were used as negative and positive controls, respectively. One-way analysis of variance (ANOVA) followed by Tukey's Honestly Significant Difference (HSD) test was used to compare treatments. Conditions sharing the same letter are not significantly different ($p > 0.05$).

Recognition of *AvrPstB48* paralogs varies across cultivars

To assess the functional redundancy of *AvrPstB48*, we tested recognition of its paralogs in the same set of wheat cultivars; Avocet S, Morocco, *T. spelta Yr5*, Gabo, and Chinese 166, using activation of the pD14 promoter as a readout. Defence

activation was detected for *AvrPstB48*_P1 and *AvrPstB48*_P2/P4 in cv. Avocet S (Figure 4a), *T. spelta Yr5* and Gabo (Supplementary Figures S2), suggesting functional similarity to *AvrPstB48*. However, *AvrPstB48*_P3 failed to activate in any tested cultivar. No induction was observed for any of the paralogs tested in Morocco (Figure 4b) and cv Chinese 166 (Supplementary Figure S2).

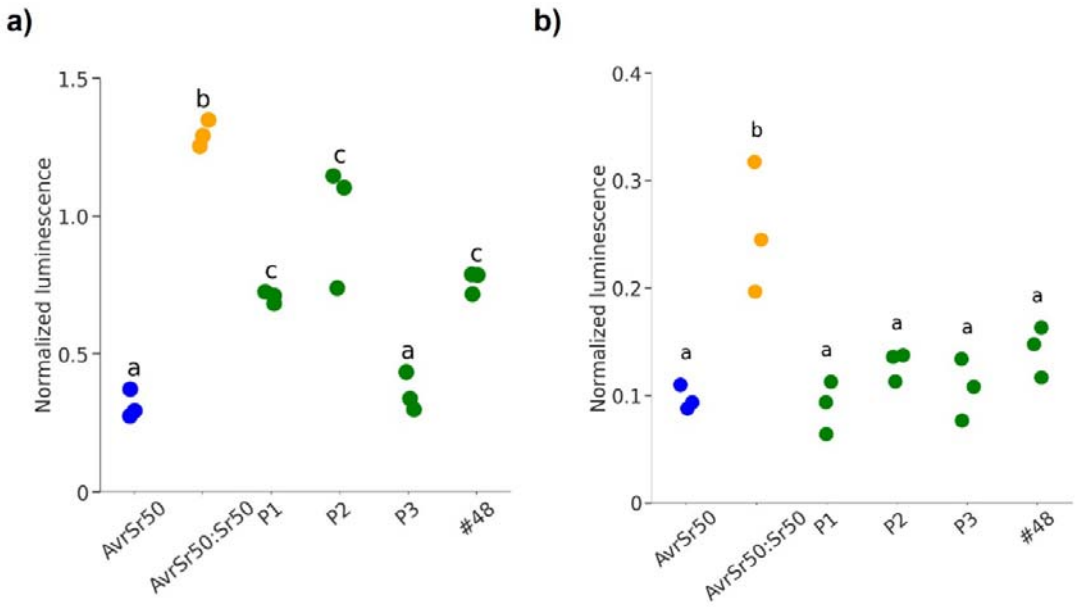

Figure 4 – Differential activation of defence reporters by *AvrPstB48* paralogs reveals genotype-dependent recognition. Normalised luminescence signals from protoplast-based defence reporter assays using the pD14 promoter construct and UBI-pRedf in **(a)** Avocet S and **(b)** Morocco. *AvrSr50* and *AvrSr50:Sr50* were included as negative and positive controls, respectively. One-way analysis of variance (ANOVA) followed by Tukey's Honestly Significant Difference (HSD) test was used to compare treatments. Conditions sharing the same letter are not significantly different ($p > 0.05$).

Lack of *AvrPstB48*_P3 recognition correlates with structural divergence

To investigate why *AvrPstB48*_P3 does not trigger defence promoter activation in Avocet S, we explored potential structural and biochemical differences among *AvrPstB48* and its paralogs. Structural predictions using AlphaFold revealed that all

paralogs adopt a broadly conserved fold (Figure 2d), suggesting the loss of recognition was not due to major misfolding. However, closer inspection revealed localised structural rearrangements unique to *AvrPstB48_P3*, particularly in surface-exposed loops potentially involved in effector recognition or host receptor interaction. One notable difference occurs at position 133, where *AvrPstB48, AvrPstB48*_P1, and *AvrPstB48*_P2 encode an aspartic acid (D), while *AvrPstB48*_P3 uniquely carries a glycine (G) at the same site (Figure 5). This substitution replaces a negatively charged residue with a small, nonpolar amino acid, potentially altering local electrostatics, stability, or protein–protein interactions. Importantly, this position is surface-exposed and represents one of the few divergent residues uniquely found in *AvrPstB48*_P3, making it a prime candidate for functional testing.

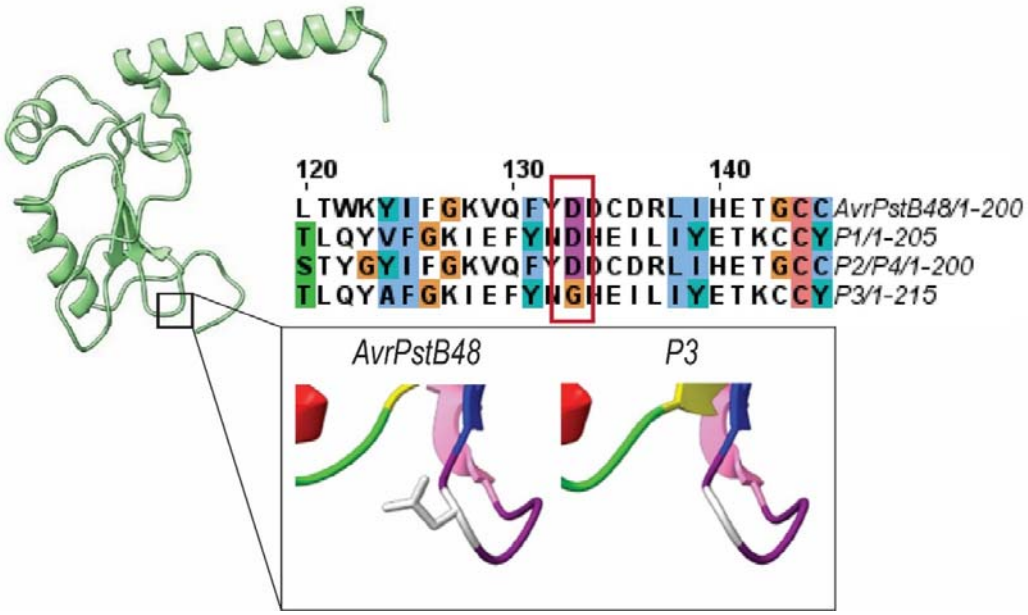

Figure 5 - AlphaFold structural predictions of *AvrPstB48* paralogs highlight amino acid variation at a conserved surface-exposed site. Predicted structures of *AvrPstB48* and *AvrPstB48*_P3 were generated using AlphaFold3. A surface-exposed position (amino acid 133) is highlighted, where *AvrPstB48*, P1, and P2/P4 encode an aspartic acid (D), while P3 uniquely carries a glycine (G). This substitution represents one of the few consistent.

Aspartic acid at position 133 is necessary but not sufficient for defence activation

To further investigate the functional significance of the amino acid variation at position 133, synthetic gene fragments were designed to encode *AvrPstB48* carrying an aspartic acid to glycine substitution (D133G), and *AvrPstB48_P3* carrying the reverse substitution (G133D). These constructs were tested for their ability to induce defence promoter activation in cv. Avocet S using the D14 promoter-luciferase reporter system in the protoplast assay. The wild-type *AvrPstB48* had previously triggered robust promoter activation in this system. However, *AvrPstB48*_D133G consistently failed to activate the defence reporter, abolishing luminescence compared to previous assays with wild-type *AvrPstB48* (Figure 6). This indicates that the D133G substitution is sufficient to disrupt recognition. Similarly, the reciprocal mutant *AvrPstB48*_P3_G133D also failed to induce defence promoter activity, suggesting that restoring a single residue is not sufficient to recover function in the structurally divergent *AvrPstB48*_P3 background.

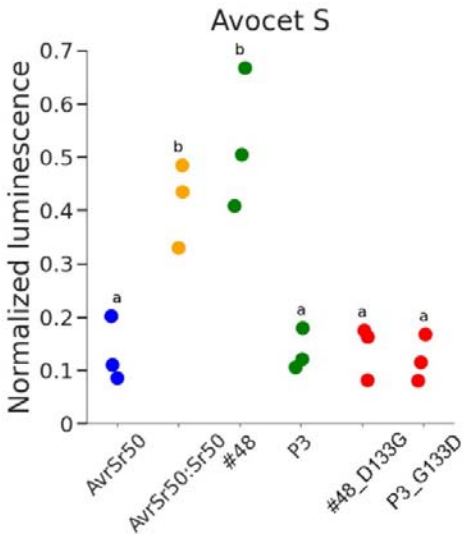

Figure 6 - Site-directed mutation at residue 133 disrupts *AvrPstB48*-mediated defence activation in wheat protoplasts. Normalised luminescence signals from protoplast-based defence reporter assays using the pD14 promoter and UBI-pRedf. One-way analysis of variance (ANOVA) followed by the Tukey Honestly Significant Difference (HSD) test was used to compare the treatments. Conditions sharing the same letter are not significantly different ($p > 0.05$).

AvrPstB48-triggered reporter activation in protoplasts does not correlate fully with *Pst* resistance *in planta*

We assessed infection outcomes using the Australian pathotype 104E137A- to evaluate whether the *AvrPstB48*-triggered reporter activation observed in wheat protoplasts corresponded to resistance *in planta*. Wheat lines previously tested in the protoplast assay were inoculated and disease severity scored at 12 days post-inoculation (dpi) using a 0–9 infection type (IT) scale. Interestingly, reporter activation in protoplasts did not consistently correlate with resistance *in planta*. While *T. spelta Yr5* and Chinese 166 exhibited full resistance (IT = 0), Gabo, Morocco, and Avocet S were highly susceptible (IT = 9), despite *AvrPstB48* triggering defence promoter activation in Gabo and Avocet S (Supplementary Figure S3).

Pathogen recognition slows infection and enhances early defence in susceptible hosts

To explore whether *Avr* recognition might influence infection dynamics even in a susceptible genotype, we compared Avocet S and Morocco, both of which are susceptible to Pst104E but with contrasting *AvrPstB48* responses. While Avocet S exhibits strong activation of a defence reporter in protoplast assays, Morocco shows no such activation, making these genotypes ideal for assessing whether *Avr*-triggered immunity affects pathogen progression *in planta*. At 8 dpi, neither line exhibited macroscopic uredospore formation. By 10 dpi, both displayed visible rust symptoms, however, Morocco developed more extensive uredospore coverage, suggesting a faster rate of fungal colonisation (Figure 7A). Confocal microscopy supported these observations, revealing more abundant and earlier hyphal growth in Morocco compared to Avocet S at 8 dpi (Figure 7B). Although both lines were heavily colonised by 10 dpi, Avocet S retained localised areas with reduced fungal presence, consistent with a delayed pathogen development.

To assess host immune responses underlying these differences, we examined callose deposition, a hallmark of plant defence. At 8 dpi, Avocet S exhibited greater callose accumulation than Morocco, particularly around infection sites (Figure 7C), and this was supported by quantitative analysis (Figure 7E). These findings indicate that the defence response in Avocet S may be linked to its ability to recognise *AvrPstB48*, consistent with protoplast assay results (Figure 1). Conversely, in Morocco, the absence of *AvrPstB48* recognition correlates with more rapid colonisation and reduced immune activation (Figure 7D).

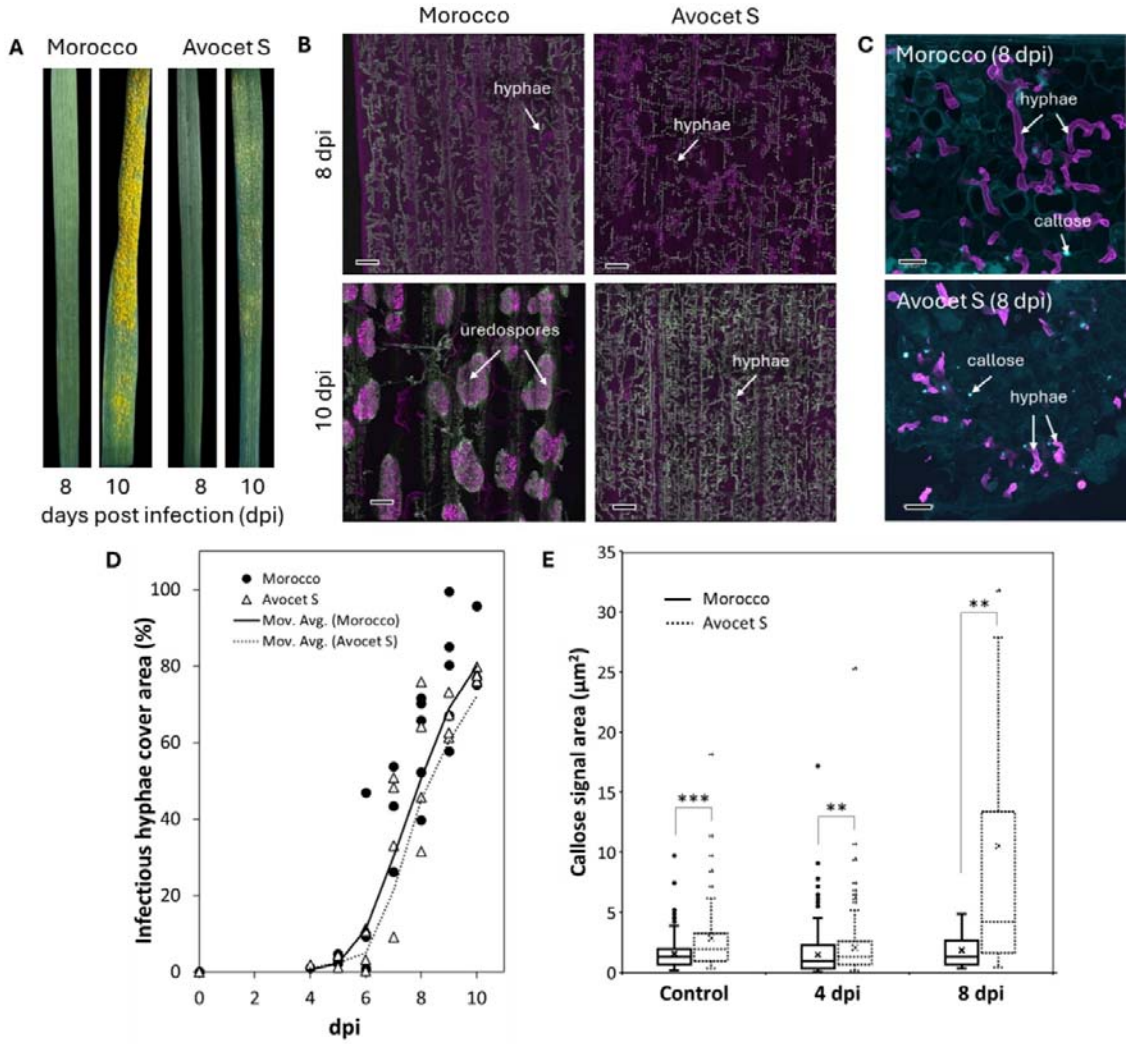

Figure 7. Infection time course analysis of *Pst*104E137A- in Morocco and Avocet S. (**A**) Leaf phenotypes at 8 and 10 days post-infection (dpi). (**B**) Representative confocal micrographs showing the extent of infection inside the leaves at 8 and 10 dpi. Magenta corresponds to propidium iodide-stained cell walls, and green to fungal structures stained with wheat germ agglutinin. Bars = 200 µm. (**C**) Representative confocal micrographs showing callose deposition (cyan) associated with infectious hyphae (magenta). Bars = 25 µm. (**D**) Infection progression and (**E**) callose deposition through time in infected leaves. Asterisks denote significant differences according to Welch's t-test at p-value < 0.01 (**) and p-value < 0.001 (***).

Discussion

Recent advances in high-quality genome assemblies of *Pst* (Wang et al., 2024), coupled with advances in effector prediction and functional genomics, have significantly enhanced our capacity to investigate host–pathogen interactions. Additionally, by integrating comprehensive effector libraries and protoplast transformation methods, we gained deeper insights into plant immunity dynamics (Arndell et al., 2024; Wilson et al., 2024). In this study, we characterised an evolutionarily conserved avirulence candidate effector, *AvrPstB48*, that triggers defence responses in wheat. Through a combination of protoplast-based assays, structural modelling and plant phenotyping, we investigated how *AvrPstB48* and its paralogs interact with wheat immune systems and influence resistance outcomes.

A central finding of this work is the genotype-dependent recognition of *AvrPstB48*. Strong defence activation was observed in wheat cultivars Avocet S, *T. spelta Yr5*, and Gabo, while others, like Morocco and Chinese 166, showed no detectable response. This supports the hypothesis that *AvrPstB48* recognition is mediated by specific *R* genes, likely encoded by NLR proteins. However, we also acknowledge the possibility that the defence activation observed in protoplasts may be, at least in part, a consequence of overexpression products inherent to the transient assay system. Nonetheless, the genotype-specific nature of the responses, the absence of activation by unrelated candidates, and the correlation with delayed disease phenotypes *in planta* all support the presence of biologically relevant recognition events. Recent studies have revealed that some stripe rust resistance genes exist as head-to-head NLR gene pairs, such as those derived from wild emmer wheat (Hu et al., 2025). Recognition variability highlights the co-evolutionary dynamics between *Pst* effectors and host immune receptors, where effectors diversify to escape

recognition, and plants evolve new surveillance mechanisms (Dodds & Rathjen, 2010; Asghar et al., 2024).

Our analysis of *AvrPstB48* paralogs revealed functional redundancy among *AvrPstB48*_P1 and *AvrPstB48*_P2/P4. These paralogs retained the ability to activate defence in cultivars that recognised *AvrPstB48*, suggesting overlapping or complementary roles. This redundancy may reflect an evolutionary strategy by *Pst* to ensure virulence through multiple, functionally convergent effectors (Mukhtar et al., 2016; Ibn-Salem et al., 2017). Such strategies have been documented in other pathosystems, underscoring the importance of assessing effector families collectively rather than in isolation (Mukhtar et al., 2011; Win et al., 2012). Moreover, the extensive genetic diversity and nuclear reassortment reported across global *Pst* populations highlight the dynamic evolutionary backdrop against which these effector diversification and redundancy events occur (Hovmøller et al., 2025)

In contrast, *AvrPstB48*_P3 failed to trigger defence responses in any tested cultivar. Structural modelling and mutational analyses revealed that a single amino acid substitution, glycine at position 133 instead of aspartic acid, possibly disrupts its recognition. This substitution probably alters the electrostatic surface properties of the protein, impairing its interaction with the host defence receptor (Tang et al., 2019). A similar effect was previously observed by Manser et al. (2021), where a mutation from aspartic acid to glycine in the Pm2a resistance protein abolished recognition of AvrPm2. This is also true in the *Pgt* effector AvrSr50, where a single amino acid substitution abolished recognition by the Sr50 receptor (Chen et al., 2017). These observations demonstrate how minor sequence changes in effectors or R genes can disrupt immune activation. Substituting aspartic acid for glycine in *AvrPstB48* abolished its defence-triggering ability, indicating that residue 133 is

necessary for recognition. However, introducing the reciprocal G133D substitution into *AvrPstB48*_P3 did not restore activity, suggesting that other polymorphisms or conformational features interfere with recognition. This illustrates that recognition is not determined by a single residue but instead results from a complex structural context, possibly involving epistatic interactions among residues that influence effector stability or surface topology (Kroj et al., 2016; Ortiz et al., 2022). These observations extend to previous findings where mutations in surface-exposed loops modulate *Avr/R* interactions (Manser et al., 2021; Ortiz et al., 2022). In our study, residue 133 is located in a predicted loop region, supporting the notion that flexible, surface-accessible regions of effectors often play critical roles in recognition. The inability of the *AvrPstB48*_P3_G133D mutant to restore defence activity implies that recognition is dependent on a combination of conserved sequence motifs and overall protein structure, rather than on single polymorphisms alone.

A significant insight from this study is the disconnect between defence activation in protoplasts and resistance phenotypes in whole plants. Although *AvrPstB48* consistently activated defence signalling in protoplast assays, cultivars like Avocet S remained fully susceptible in foliar infection assays. This discrepancy underscores the complexity of immune responses *in planta*, where effectors may be recognised but downstream responses are suppressed (Saur et al., 2019; Wu & Derevnina, 2023). We propose that *AvrPstB48* is recognised in some wheat cultivars, triggering early immune responses, but this recognition is masked by other *Pst* effectors with suppressor functions. Comparative infection assay between Avocet S and Morocco support this hypothesis. Both cultivars are susceptible to Pst104E, yet only Avocet S recognised *AvrPstB48* in protoplasts. *In planta*, Avocet S exhibited delayed disease progression, reduced mycelial growth, and increased callose deposition compared to

Morocco. While the underlying mechanisms remain to be fully resolved, the phenotypes observed in Avocet S are consistent with a transient defence response that may be associated with *AvrPstB48*, followed by immune suppression that ultimately allows pathogen proliferation. Also, Avocet S is known to carry at least one functional resistance gene capable of recognising avirulent isolates of *Pst* (Nazari & Amil, 2013). The concept of effector-triggered susceptibility (ETS), wherein suppressor effectors negate recognition-triggered defences, has been previously reported (Zambino et al., 2000; Zhang et al., 2023) and may also be present in the *Pst*-wheat interaction.

CONCLUSION

This study provides a comprehensive characterisation of *AvrPstB48*, an avirulence candidate effector in *Pst*, revealing its capacity to elicit genotype-specific immune responses in wheat. Through an integrated approach combining high-throughput protoplast assays, structural modelling, and *in planta* phenotyping, we demonstrate that *AvrPstB48* recognition alone is insufficient to confer effective resistance. Instead, our findings support a model in which *Avr*-triggered immune responses can be actively suppressed, resulting in delayed or incomplete resistance.

The functional divergence among *AvrPstB48* paralogs highlights how discrete structural changes can abolish recognition. This underscores the importance of evaluating effector structure holistically, considering both conserved motifs and the spatial arrangement of surface-exposed residues. The inability of cultivars like Avocet S to mount effective resistance, despite recognising *AvrPstB48,* illustrates the limitations of reductionist systems and the need to interpret *Avr/R* interactions within the broader context of the pathogen effector collection.

Together, these findings reinforce the complex nature of the plant immune landscape, shaped by a dynamic balance of recognition and suppression. They emphasise the need for functional assays that account for multi-effector interactions and the role of suppressors in determining resistance outcomes.

Data availability

All supporting data are also available on Zenodo (doi: 10.5281/zenodo.15845412, link: 10.5281/zenodo.15845412).

References

1. Abramson, J., Adler, J., Dunger, J., Evans, R., Green, T., Pritzel, A., Ronneberger, O., Willmore, L., Ballard, A.J., Bambrick, J., Bodenstein, S.W., Evans, D.A., Hung, C.C., O'Neill, M., Reiman, D., Tunyasuvunakool, K., Wu, Z., Žemgulytė, A., Arvaniti, E., Beattie, C., Bertolli, O., Bridgland, A., Cherepanov, A., Congreve, M., Cowen-Rivers, A.I., Cowie, A., Figurnov, M., Fuchs, F.B., Gladman, H., Jain, R., Khan, Y.A., Low, C.M.R., Perlin, K., Potapenko, A., Savy, P., Singh, S., Stecula, A., Thillaisundaram, A., Tong, C., Yakneen, S., Zhong, E.D., Zielinski, M., Žídek, A., Bapst, V., Kohli, P., Jaderberg, M., Hassabis, D., Jumper, J.M. 2024. Addendum: Accurate structure prediction of biomolecular interactions with AlphaFold 3. Nature. 636(8042): E4.

2. Amezrou, R., Audeon, C., Compain, J., Gelisse, S., Ducasse, A., Saintenac, C., Lapalu, N., Louet, C., Orford, S., Croll, D. et al. 2023. A secreted protease-like protein in *Zymoseptoria tritici* is responsible for avirulence on Stb9 resistance gene in wheat. PLoS Pathog. 19: e1011376.

3. Arndell, T., Chen, J., Sperschneider, J., Upadhyaya, N.M., Blundell, C., Niesner, N., Outram, M.A., Wang, A., Swain, S., Luo, M., Ayliffe, M.A., Figueroa, M., Vanhercke, T., and Dodds, P.N. 2023. Pooled effector library screening in protoplasts rapidly identifies novel *Avr* genes. Nat. Plants 10: 572–580.

4. Asghar, R., Wu, N., Ali, N., Wang, Y., Akkaya, M. (2025). Computational studies reveal structural characterization and novel families of *Puccinia striiformis* f. sp. *tritici* effectors. PLoS Comput. Biol. 21: e1012503.

5. Bourras, S., Kunz, L., Xue, M., Praz, C.R., Muller, M.C., Kälin, C., Schläfli, M., Ackermann, P., Flückiger, S., Parlange, F., et al. 2019. The *Avr*Pm3-Pm3 effector-NLR interactions control both race-specific resistance and host specificity of cereal mildews on wheat. Nat. Commun. 10: 2292.

6. Chang, J., Mapuranga, J., Li, R., Zhang, Y., Shi, J., Yan, H., and Yang, W. 2024. Wheat leaf rust fungus effector protein Pt1641 is avirulent to TcLr1. Plants (Basel) 13: 2255.

7. Chen, J., Upadhyaya, N.M., Ortiz, D., Sperschneider, J., Li, F., Bouton, C., Breen, S., Dong, C., Xu, B., Zhang, X., et al. 2017. Loss of *Avr*Sr50 by somatic exchange in stem rust leads to virulence for Sr50 resistance in wheat. Science 358: 1607–1610.

8. Chen, R., Chen, J., Outram, M.A., Powell, O.R., Arndell, T., Gajendiran, K., Wang, Y.L., Ayliffe, M.A., Blundell, C., Figueroa, M., Sperschneider, J., Vanhercke, T., Tang, D., Xu, Y., Zhong, G., Gardener, C., Yu, G., Gourdoupis, S., Jaremko, Ł., Matny, O., Steffenson, B.J., Boshoff, W.H.P., Meyer, W.B., Arold, S.T., Dodds, P.N., and Wulff, B.B.H. 2024. A wheat tandem kinase sensor activates an NLR helper to trigger immunity. Science 387: 1402-1408.

9. Cui Z, Shen S, Meng L, Sun X, Jin Y, Liu Y, Liu D, Ma L, Wang H. 2024. Evasion of wheat resistance gene Lr15 recognition by the leaf rust fungus is attributed to the coincidence of natural mutations and deletion in AvrLr15 gene. Mol. Plant Pathol. 25: e13490.

10. Dodds, P.N., and Rathjen, J.P. 2010. Plant immunity: Towards an integrated view of plant-pathogen interactions. Nat. Rev. Genet. 11: 539–548.

11. Engler C, Youles M, Gruetzner R, Ehnert TM, Werner S, Jones JD, Patron NJ, Marillonnet S. 2014. A golden gate modular cloning toolbox for plants. ACS Synth Biol. 3: 839-43.

12. González-Grandío, E., Demirer, G.S., Ma, W., Brady, S., Landry, M.P. 2021. A ratiometric dual color luciferase reporter for fast characterization of transcriptional regulatory elements in plants. ACS Synth. Biol. 10: 2763–2766.

13. Hovmøller, M.S., Walter, S., and Justesen, A.F. 2010. Escalating threat of wheat rusts. Science 329: 369.

14. Hovmøller MS, Thach T, Rodriguez-Algaba J, Hansen JG, Meyer M, Hodson D, Nazari K, Park RF, Tam R, Möller M, Schwessinger B, Rathjen JP, Silva P, Riella V, Justesen AF. 2025. Long-term surveillance suggests multiple hybridization events by nuclear reassortment and accelerated intercontinental spread of wheat yellow rust. bioRxiv 2025.05.22.655633. doi: 10.1101/2025.05.22.655633

15. Hu, Y., Li, M., Li, Y. et al. 2025. A head-to-head NLR gene pair from wild emmer confers stripe rust resistance in wheat. Nat Genet 57: 1543–1552.

16. Ibn-Salem, J., Muro, E.M., Andrade-Navarro, M.A. 2017. Co-regulation of paralog genes in the three-dimensional chromatin architecture. Nucleic Acids Res. 45: 81-91.

17. Jumper, J., Evans, R., Pritzel, A., Green, T., Figurnov, M., Ronneberger, O., Tunyasuvunakool, K., Bates, R., Žídek, A., Potapenko, A., et al. 2021. Highly accurate protein structure prediction with AlphaFold. Nature, 596: 583–589.

18. Karki SJ, Pilo P, Lawless C, Mastrodimos N, Tiley AMM, Burke J, Feechan A. The Zymoseptoria tritici effector Zt-11 contributes to aggressiveness in wheat. PLoS One. 19: e0313859.

19. Katoh K, Standley DM. 2013. MAFFT multiple sequence alignment software version 7: improvements in performance and usability. Mol. Biol. Evol. 30: 772-80.

20. Kroj, T., Chanclud, E., Michel-Romiti, C., Grand, X., Morel, J.B. 2016. Integration of decoy domains derived from protein targets of pathogen effectors into plant immune receptors is widespread. New Phytol. 21: 618-26.

21. Li H. 2018. Minimap2: pairwise alignment for nucleotide sequences. Bioinformatics. 34: 3094–3100.

22. Li J, Ren J, Dai W, Stubenrauch C, Finn RD, Wang J. 2024. Fungtion: A Server for Predicting and Visualizing Fungal Effector Proteins. J. Mol. Biol. 436: 168613.

23. Liu, C., Pedersen, C., Schultz-Larsen, T., Aguilar, G.B., Madriz-Ordeñana, K., Hovmøller, M.S., Thordal-Christensen, H. 2016. The stripe rust fungal effector PEC6 suppresses pattern-triggered immunity in a host species-independent manner and interacts with adenosine kinases. New Phytol. doi:10.1111/nph.14034

24. Love, M.I., Huber, W., Anders, S. 2014. Moderated estimation of fold change and dispersion for RNA-seq data with DESeq2. Genome Biol. 15: 550.

25. Lubega J, Figueroa M, Dodds PN, Kanyuka K. 2024. Comparative Analysis of the Avirulence Effectors Produced by the Fungal Stem Rust Pathogen of Wheat. Mol. Plant Microbe Interact. 37: 171-178.

26. Manser, B., Koller, T., Praz, C.R., Roulin, A.C., Zbinden, H., Arora, S., Steuernagel, B., Wulff, B.B.H., Keller, B., Sánchez-Martín, J. 2021. Identification of specificity-defining amino acids of the wheat immune receptor Pm2 and powdery mildew effector AvrPm2. Plant J. 106: 993-1007.

27. Meile, L., Croll, D., Brunner, P. C., Plissonneau, C., Hartmann, F. E., McDonald, B. A., Sánchez-Vallet, A. 2018. A fungal avirulence factor encoded in a highly plastic genomic region triggers partial resistance to septoria tritici blotch. New Phytol. 219: 1048-1061.

28. Meng, E.C., Goddard, T.D., Pettersen, E.F., Couch, G.S., Pearson, Z.J., Morris, J.H., Ferrin, T.E. 2023. UCSF ChimeraX: Tools for structure building and analysis. Protein Sci. 32: e4792.

29. Mukhtar, M.S., Carvunis AR, Dreze M, Epple P, Steinbrenner J, Moore J, Tasan M, Galli M, Hao T, Nishimura MT, Pevzner SJ, Donovan SE, Ghamsari L, Santhanam B, Romero V, Poulin MM, Gebreab F, Gutierrez BJ, Tam S, Monachello D, Boxem M, Harbort CJ, McDonald N, Gai L, Chen H, He Y; European Union Effectoromics Consortium; Vandenhaute J, Roth FP, Hill DE, Ecker JR, Vidal M, Beynon J, Braun P, Dangl JL. 2011. Independently evolved virulence effectors converge onto hubs in a plant immune system network. Science. 333: 596-601.

30. Mukhtar, M.S., McCormack, M.E., Argueso, C.T., Pajerowska-Mukhtar, K.M. 2016. Pathogen Tactics to Manipulate Plant Cell Death. Curr. Biol. 26: R608-R619.

31. Nazari K, El Amil R. 2013. First Report of Resistance of Wheat Line Avocet 'S' to Stripe Rust Caused by *Puccinia striiformis* f. sp*. tritici* (*Pst*) in Syria. Plant Dis. 97: 996.

32. Norman M, Bariana H, Bansal U, Periyannan S. The Keys to Controlling Wheat Rusts: Identification and Deployment of Genetic Resistance. Phytopathology. 113: 667-677.

33. Ortiz, D., Chen, J., Outram, M. A., Saur, M. L., Upadhyaya, N. M., Mago, R., Ericsson, D. J., Cesari, S., Chen, C., Williams, S. J., & Dodds, P. N. 2022. The stem rust effector protein *Avr*Sr50 escapes Sr50 recognition by a substitution in a single surface-exposed residue. New Phytol. 234: 592–606.

34. Outram, M. A., Chen, J., Broderick, S., Li, Z., Aditya, S., Tasneem, N., Arndell, T., Blundell, C., Ericsson, D. J., Figueroa, M., Sperschneider, J., Dodds, P. N., Williams, S. J. (2024). *Avr*Sr27 is a zinc-bound effector with a modular structure important for immune recognition. New Phytol. 243: 314-329.

35. Praz CR, Bourras S, Zeng F, Sanchez-Martın J, Menardo F, Xue M, Yang L, Roffler S, B€oni R, Herren G et al. 2017. *Avr*Pm2 encodes an RNaselike avirulence effector which is conserved in the two different specialized forms of wheat and rye powdery mildew fungus. New Phytol. 213: 1301–1314.

36. Ramírez-Zavaleta, C.Y., García-Barrera, L.J., Rodríguez-Verástegui, L.L., Arrieta-Flores, D., Gregorio-Jorge, J. 2022. An Overview of PRR- and NLR-

Mediated Immunities: Conserved Signaling Components across the Plant Kingdom That Communicate Both Pathways. Int. J. Mol. Sci. 23: 12974.

37. Redkar A, Jaeger E, Doehlemann G. 2018. Visualization of growth and morphology of fungal hyphae in planta using WGA-AF488 and propidium iodide co-staining. Bio-Protocol. 8: e2942.

38. Rhodes, J., Zipfel, C., Jones, J.D.G., Ngou, B.P.M. 2022. Concerted actions of PRR- and NLR-mediated immunity. Essays Biochem. 66: 501-511.

39. Running, K.L.D., Faris, J.D. 2024. Rapid Cloning of Disease Resistance Genes in Wheat. In: Appels, R., Eversole, K., Feuillet, C., Gallagher, D. (eds) The Wheat Genome. Compendium of Plant Genomes. Springer, Cham.

40. Salcedo A, Rutter W, Wang S, Akhunova A, Bolus S, Chao S, Anderson N, De Soto MF, Rouse M, Szabo L, Bowden RL, Dubcovsky J, Akhunov E. 2017. Variation in the *Avr*Sr35 gene determines Sr35 resistance against wheat stem rust race Ug99. Science. 358: 1604-1606.

41. Schwessinger, B., Sperschneider, J., Cuddy, W.S., Garnica, D.P., Miller, M.E., Taylor, J.M., Dodds, P.N., Figueroa, M., Park, R.F., Rathjen, J.P. 2018. A Near-Complete Haplotype-Phased Genome of the Dikaryotic Wheat Stripe Rust Fungus *Puccinia striiformis* f. sp. *tritici* Reveals High Interhaplotype Diversity. mBio 9: e02275-17

42. Saur IML, Bauer S, Lu X, Schulze-Lefert P. 2019. A cell death assay in barley and wheat protoplasts for identification and validation of matching pathogen *AVR* effector and plant NLR immune receptors. Plant Methods. 15: 118.

43. Shen, S., Wang, F., Cui, Z. et al. 2024. *Puccinia triticina* avirulence protein AvrLr21 directly interacts with wheat resistance protein Lr21 to activate wheat immune response. Commun. Biol. 7: 1170.

44. Ramachandran, S.R., Yin, C., Kud, J., Tanaka, K., Mahoney, A.K., Xiao, F., Hulbert, S.H. 2017. Effectors from Wheat Rust Fungi Suppress Multiple Plant Defense Responses. Phytopathology. 107: 75-83.

45. Tam, R., Möller, M., Luo, R., Luo, Z., Jones, A., Periyannan, S., Rathjen, J.P., Schwessinger, B. 2025. Long-read genomics reveal extensive nuclear-specific evolution and allele-specific expression in a dikaryotic fungus. Genome Res. 11: gr.280359.124.

46. Tang, J., Wang, Y., Yin, W., Dong, G,, Sun, K., Teng, Z., Wu, X., Wang, S., Qian, Y., Pan, X., Qian, Q., Chu, C. 2019. Mutation of a Nucleotide-Binding Leucine-Rich Repeat Immune Receptor-Type Protein Disrupts Immunity to Bacterial Blight. Plant Physiol. 181: 1295-1313.

47. Todd, J.N.A., Carreón-Anguiano, K.G., Islas-Flores, I., Canto-Canché, B. 2022. Microbial Effectors: Key Determinants in Plant Health and Disease. Microorganisms. 10: 1980.

48. Shen, S., Wang, F., Cui, Z. Yuan, S., Meng, L., Liu, D., Ma, L., Wang, H. 2024. *Puccinia triticina* avirulence protein *Avr*Lr21 directly interacts with wheat resistance protein Lr21 to activate wheat immune response. Commun. Biol. 7: 1170.

49. Upadhyaya, N.M., Mago, R., Panwar, V., Hewitt, T., Luo, M., Chen, J., Sperschneider, J., Nguyen-Phuc, H., Wang, A., Ortiz, D., Hac, L., Bhatt, D., Li, F., Zhang, J., Ayliffe, M., Figueroa, M., Kanyuka, K., Ellis, J.G., Dodds, P.N. 2021.

Genomics accelerated isolation of a new stem rust avirulence gene-wheat resistance gene pair. Nat Plants. 7: 1220-1228.

50. Waheed, A., Haxim, Y., Islam, W., Kahar, G., Liu, X., Zhang, D. 2022. Role of pathogen's effectors in understanding host-pathogen interaction. Biochim. Biophys. Acta Mol. Cell. Res. 1869: 119347.

51. Wang, J., Chen, T., Tang, Y., Zhang, S., Xu, M., Liu, M., Zhang, J., Loake, G.J., Jiang, J. (2023). The Biological Roles of *Puccinia striiformis* f. sp. *tritici* Effectors during Infection of Wheat. Biomolecules. 13: 889.

52. Wang, J., Xu, Y., Peng, Y. et al. 2024. A fully haplotype-resolved and nearly gap-free genome assembly of wheat stripe rust fungus. Sci. Data 11: 508.

53. Wilson, S., Dagvadorj, B., Tam, R., Schwessinger, B. (n.d.). Wheat protoplast preparation and transformation (Version 1). protocols.io. https://dx.doi.org/10.17504/protocols.io.q26g7r3zkvwz/v1

54. Wilson, S., Dagvadorj, B., Tam, R., Murphy, L., Schulz-Kroenert, S., Heng, N., Crean, E., Greenwood, J., Rathjen, J.P., Schwessinger, B. 2024. Multiplexed effector screening for recognition by endogenous resistance genes using positive defense reporters in wheat protoplasts. New Phytol, 241: 2621-2636.

55. Win J, Chaparro-Garcia A, Belhaj K, Saunders DG, Yoshida K, Dong S, Schornack S, Zipfel C, Robatzek S, Hogenhout SA, Kamoun S. 2012. Effector biology of plant-associated organisms: concepts and perspectives. Cold Spring Har. Symp. Quant. Biol. 77: 235–247.

56. Wu CH, Derevnina L. 2023. The battle within: How pathogen effectors suppress NLR-mediated immunity. Curr. Opin. Plant Biol. 74: 102396.

57. Wu, N., Ozketen, A.C., Cheng, Y., Jiang, W., Zhou, X., Zhao, X., Guan, Y., Xiang, Z., Akkaya, M.S. 2022. *Puccinia striiformis* f. sp. *tritici* effectors in wheat immune responses. Front. Plant Sci. 13: 1012216.

58. Xia, C., Lei, Y., Wang, M., Chen, W., Chen, X. 2020. An avirulence gene cluster in the wheat stripe rust pathogen (*Puccinia striiformis* f. sp*. tritici*) identified through genetic mapping and whole-genome sequencing of a sexual population. mSphere 5: 10.1128/msphere.00128-20.

59. Yu, D.S., Outram, M.A., Smith, A., McCombe, C.L., Khambalkar, P.B., Rima, S.A., Sun, X., Ma, L., Ericsson, D.J., Jones, D.A., Williams, S.J. 2024. The structural repertoire of *Fusarium oxysporum* f. sp. *lycopersici* effectors revealed by experimental and computational studies. Elife.12: RP89280.

60. Zambino, P.J., Kubelik, A.R. Szabo, L.J. 2000. Gene Action and Linkage of Avirulence Genes to DNA Markers in the Rust Fungus *Puccinia graminis*. Phytopathology. 90: 819-826.

61. Zhang, X., Farah, N., Rolston, L., Ericsson, D.J., Catanzariti, A.M., Bernoux, M., Ve, T., Bendak, K., Chen, C., Mackay, J.P., Lawrence, G.J., Hardham, A., Ellis, J.G., Williams, S.J., Dodds, P.N., Jones, D.A., Kobe, B. 2018. Crystal structure of the *Melampsora lini* effector AvrP reveals insights into a possible nuclear function and recognition by the flax disease resistance protein. P. Mol. Plant Pathol. 19: 1196-1209.

62. Zhang, G.S., Liu, W., Wang, L., Ju, M., Tian, X.X., Du, Z.M., Kang, Z., Zhao, J.. 2023. Genetic characteristics and linkage of virulence genes of the *Puccinia striiformis* f. sp. *tritici* TSA-6 Isolate to *Yr5* Host Resistance. Plant Disease. 107: 688-700.

63. Zhao, M., Wang, J., Ji, S., Chen, Z., Xu, J., Tang, C., Chen, S., Kang, Z. Wang, X. 2018. Candidate Effector *Pst*_8713 Impairs the Plant Immunity and Contributes to Virulence of *Puccinia striiformis* f. sp. *tritici*. Front. Plant Sci. 9: 1294.

64. Zheng, P., Liu, M., Pang, L., Sun, R., Yao, M., Wang, X., Kang, Z., & Liu, J. 2023. Stripe rust effector *Pst*21674 compromises wheat resistance by targeting transcription factor TaASR3. Plant Physiol. 193: 2806-2824.

65. Zhong, Z., Marcel, T.C., Hartmann, F.E., Ma, X., Plissonneau, C., Zala, M., Ducasse, A., Confais, J., Compain, J., Lapalu, N., Amselem, J., McDonald, B.A., Croll, D., Palma-Guerrero, J. 2017. A small secreted protein in *Zymoseptoria tritici* is responsible for avirulence on wheat cultivars carrying the Stb6 resistance gene. New Phytol. 214, 619-631

Supplementary Figures

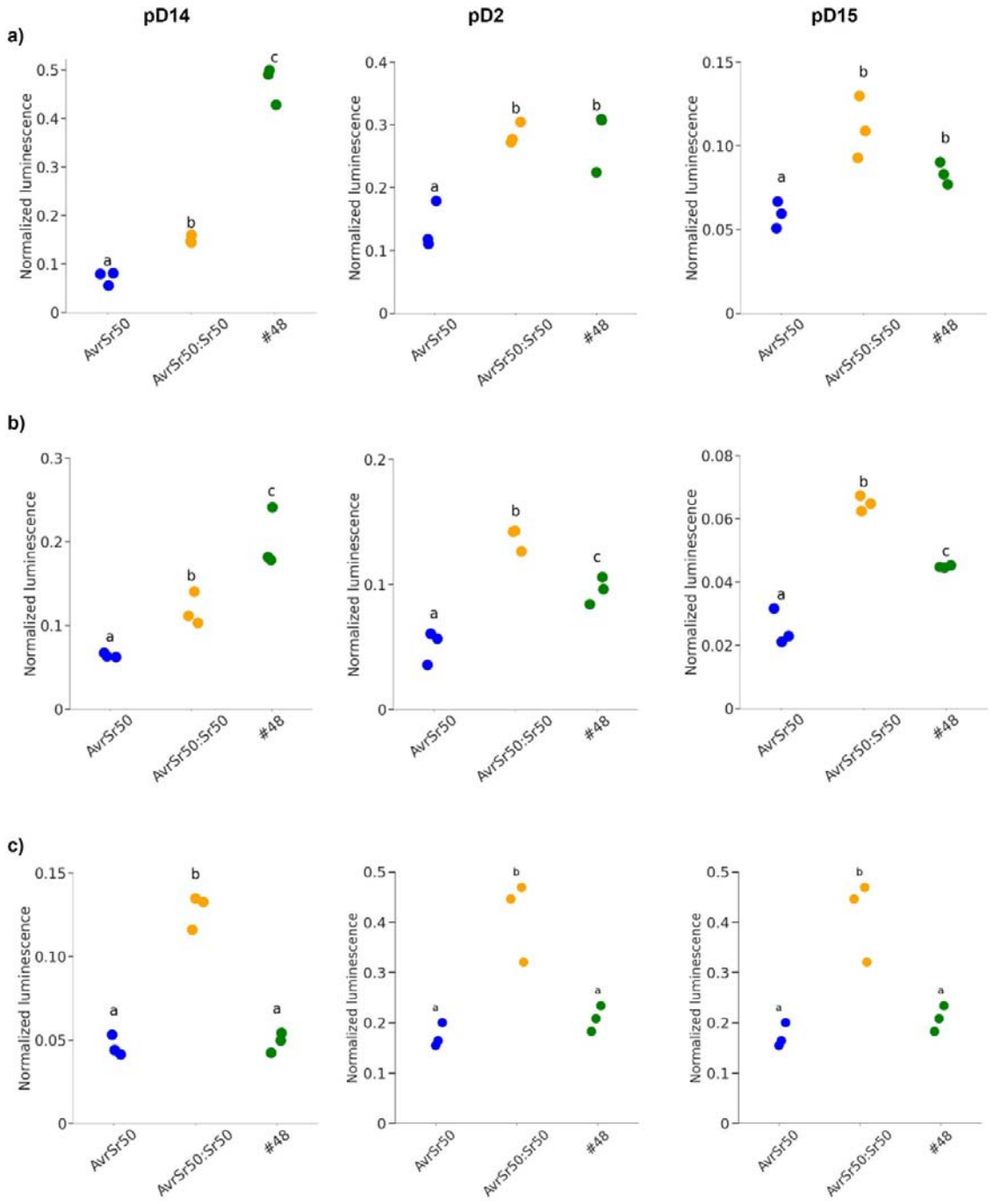

Figure S1 - Differential activation of defence reporters by *AvrPstB48* reveals genotype-dependent recognition. Normalised luminescence signals from protoplast-based defence reporter

assays using three promoter constructs (pD14, pD2, pD15) and UBI-pRedf in **(a)** Triticum spelta *Yr5*, **(b)** Gabo and **(c)** Chinese 166. AvrSr50 and AvrSr50:Sr50 were used as negative and positive controls, respectively. One-way analysis of variance (ANOVA) followed by Tukey's Honestly Significant Difference (HSD) test was used to compare treatments. Conditions sharing the same letter are not significantly different ($p > 0.05$).

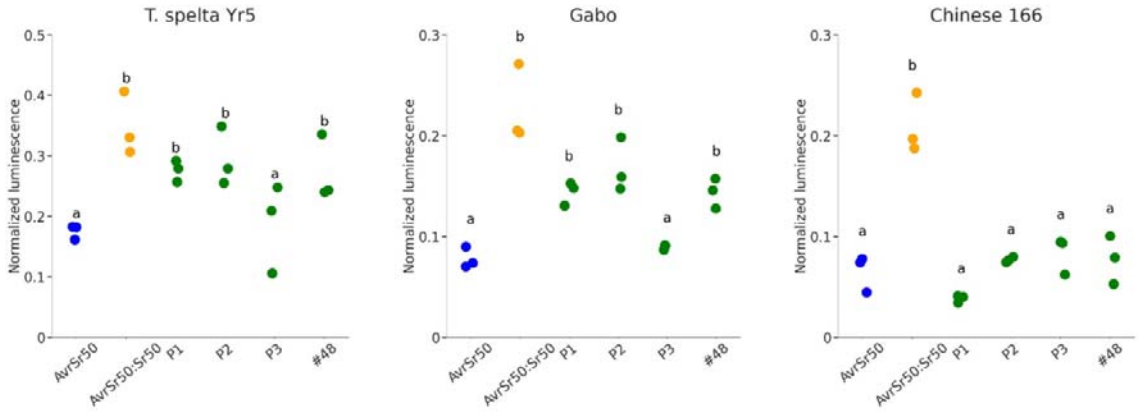

Figure S2 - Differential activation of defence reporters by *AvrPstB48* paralogs reveals genotype-dependent recognition. Normalized luminescence signals from protoplast-based defence reporter assays using the pD14 promoter construct and UBI-pRedf in **(a)** Triticum spelta *Yr5*, **(b)** Gabo and **(c)** Chinese 166. AvrSr50 and AvrSr50:Sr50 were included as negative and positive controls, respectively. One-way analysis of variance (ANOVA) followed by Tukey's Honestly Significant Difference (HSD) test was used to compare treatments. Conditions sharing the same letter are not significantly different ($p > 0.05$).

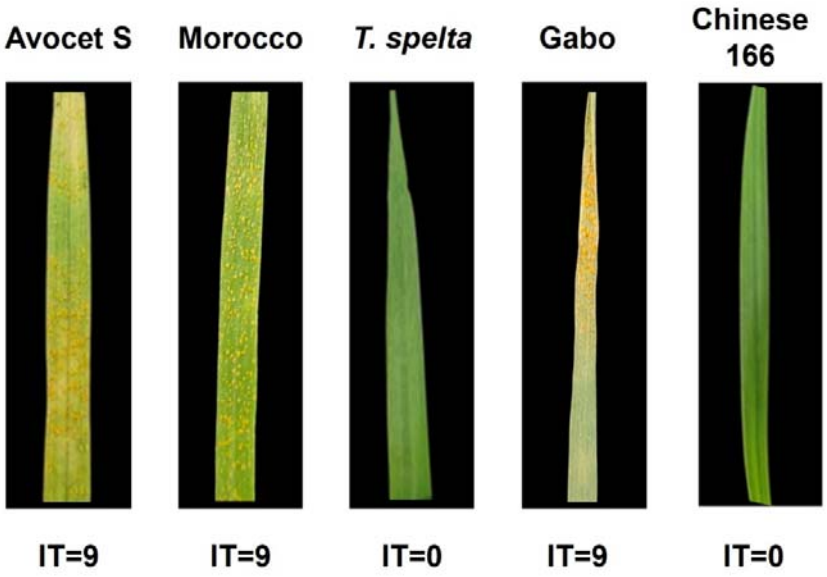

Figure S3 – Infection types (IT) on a 0-9 scale for the isolate 104E137A- inoculated on the wheat cultivars *Triticum spelta Yr5*, Avocet S, Chinese 166, Morocco and Gabo. 0: no visible disease symptoms (immune), 1: minor chlorotic and necrotic flecks, 2: chlorotic and necrotic flecks without sporulation, 3–4: chlorotic and necrotic areas with limited sporulation, 5–6: chlorotic and necrotic areas with moderate sporulation, 7: abundant sporulation with moderate chlorosis, 8–9: abundant and dense sporulation without notable chlorosis and necrosis.

Supplementary Tables

Table S1 - Comparative sequence alignment and AlphaFold modelling metrics for AvrPstB48 and paralogS (P1, P2/P4, P3). The AlphaFold metrics include ipTM (interface predicted TM-score) and pTM (predicted TM-score), which estimate confidence in the predicted structures and inter-domain orientations, with higher values indicating greater reliability. The “Zn” column indicates whether zinc ions were included during modelling, as zinc can stabilise cysteine-rich proteins and influence predicted folding.

Table S2 – Primers (DB34 and DB35) to confirm the presence of Avr candidate inserts in transformed *E. coli* colonies.

Table S3 - List of plasmids.

Table 4 - Resume of Avirulence (Avr) screening in wheat protoplasts of various differential wheat lines to *Puccinia striiformis* f. sp*. tritici* (*Pst*) Pst104E137A-infection in a protoplast-based defence reporter assay.

Table S4 – **Avirulence (*Avr*) screening results in wheat protoplasts and *in vivo* infection assays**. Response of various differential wheat lines to *Puccinia striiformis* f. sp. *tritici* (*Pst*) *Pst*104E137A-infection and the induction of *AvrPstB48* in a protoplast-based defence reporter assay. "*Pst*-resistant gene" refers to the known Yr gene(s) present in each line. "*AvrPstB48* induction" indicates whether candidate *AvrPstB48* triggered a defence response (+) or not (-) in the protoplast assay. "*Pst*infection" represents the *in vivo* susceptibility (+) or resistance (-) of the wheat lines to *Pst*, (ns) indicates that infection data are not available for that line.